Characterization on Improved Effective Mobility of Pentacene Organic Field-Effect Transistors Using Graphene Electrodes

Sangchul Lee[1], Gunho Jo[2], Seok-Ju Kang[3], Woojin Park[3], Yung Ho Kahng[4],
Dong-Yu Kim[1,3], Byoung Hun Lee[1,3], and Takhee Lee[2]*

[1]*Department of Nanobio Materials and Electronics, Gwangju Institute of Science and Technology, Gwangju 500-712, Korea*
[2]*Department of Physics and Astronomy, Seoul National University, Seoul 151-747, Korea*
[3]*School of Materials Science and Engineering, Gwangju Institute of Science and Technology, Gwangju 500-712, Korea*
[4]*Research Institute for Solar and Sustainable Energies, Gwangju Institute of Science and Technology, Gwangju 500-712, Korea*

Pentacene organic field-effect transistors (OFETs) with multilayer graphene (MLG) films as the source and drain electrodes were fabricated. Pentacene OFETs with MLG electrodes showed significantly enhanced electrical property compared to devices with typically used Au electrodes because MLG electrode yields lower contact resistance and lower barrier height. Specifically, the pentacene OFETs with graphene electrodes exhibited increased output current by more than tenfold, high mobility as $0.4 \, \text{cm}^2 \, \text{V}^{-1} \, \text{s}^{-1}$, and high on/off current ratio of 10^7. Our study may be useful for the development of organic transistors that are capable of producing improved performances.

© 2012 The Japan Society of Applied Physics

1. Introduction

In the past few years, a number of research groups have been trying to considerably enhance the performance of organic field-effect transistors (OFETs).[1–3] Among such efforts, pentacene which is a small molecule aromatic hydrocarbon has been used to fabricate high performance OFET due to low cost thin film device applications.[4,5] However, for practical applications, the performance of pentacene OFETs needs to be more improved. To enhance the device performance, one can consider many factors in OFETs such as gate dielectric, interface of dielectric and organic semiconductor, ohmic contacts at charge injection electrode to the organic semiconductor, etc. Among them, one of the simple approaches is to choose better source and drain electrodes for more efficient charge injection into active organic channel.[6,7]

In the meantime, graphene has gained high attention as an alternative electrode material for organic devices due to its advantageous property such as high transparency, flexibility, and high charge carrier mobility.[8,9] In particular, it has been demonstrated that the multilayer graphene (MLG) electrodes produce low contact resistance due to a lower charge-injection barrier to the pentacene active channel as compared to the traditional Au electrode.[10] Therefore, graphene may play a promising candidate for electrode application in many types of electronic and optical devices.[11,12]

Herein, we present enhanced performance of pentacene OFETs with multilayer graphene electrodes compared to pentacene OFETs with conventional Au electrodes. The electrical performance of pentacene OFETs with graphene electrodes was significantly improved with decreased contact resistance and enhanced charge injection, which results in improved mobility. We also investigated and compared the temperature-dependent mobility property of pentacene OFETs with graphene electrodes and with Au electrodes.

2. Experimental Procedure

A schematic and optical image of the bottom-contact pentacene OFETs are shown in Fig. 1(a). The transistors were fabricated on a heavily doped Si (p^{++} Si) wafer, which is used as a common back-gate electrode. A 300 nm thick SiO_2 layer was used as the gate dielectric. We employed the MLG film as source and drain electrodes. MLG was synthesized by a chemical vapor deposition on nickel films. MLG film was transferred and patterned on a SiO_2/Si wafer. Subsequently, the patterned MLG electrodes were coated with poly(methyl methacrylate) (PMMA) to be easily separated from SiO_2 substrate. The PMMA-coated MLG electrodes were detached by etching of SiO_2 layer with buffered oxide etchant. Then, the detached MLG electrodes were transferred to the octadecyltrichlorosilane (OTS)-treated SiO^2/p^{++} Si device substrate. Finally, 60 nm thick pentacene was deposited on top of the MLG electrodes and the dielectric layer by vacuum thermal evaporation. So, the devices are bottom-contact OFETs. The pentacene was used as received (from Sigma Aldrich) without further purification. The channel length and width of the pentacene OFETs were 50 μm and 1 mm, respectively. We also fabricated the similar devices with Au source and drain electrodes for the comparison with the graphene-electrode devices. The details of the graphene growth and OFET device fabrication have been reported elsewhere.[10]

The current–voltage curves were measured using a Keithley 4200-SCS parameter analyzer connected to a probe station inside a N_2-filled glove box, and the temperature dependent transport properties were measured with HP4155A semiconductor parameter analyzer connected to a cryostat (Janis ST-100) while the temperature was varied from 300 to 180 K with 10 K intervals by flowing liquid nitrogen into the sample holder in the vacuum chamber.

3. Result and Discussion

Figure 1(b) is the optical image of MLG film transferred to a SiO_2/Si substrate. The grain size of MLG is more than 10 μm. MLG film appears to be composed of thick and thin regions. Figure 1(c) shows the Raman spectra measured from two marked positions [cross marked with label (i) and (ii)] shown in Fig. 1(b). The bottom plot in Fig. 1(c) displays the typical features of monolayer graphene and the top plot in Fig. 1(c) indicates multilayer graphene. Both
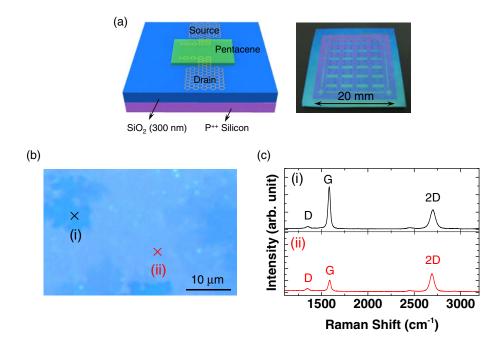
*E-mail address: tlee@snu.ac.kr

Fig. 1. (Color online) (a) Schematic (left) and a real image (right, $2\,cm \times 2\,cm$) of graphene-electrode pentacene OFET. (b) An optical image of a multilayer graphene film on SiO_2 substrate. (c) Raman spectra obtained from the positions marked in (b).
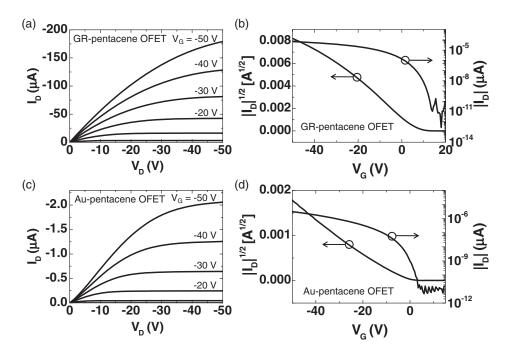

Fig. 2. (a, c) I_D–V_D plots measured at V_G ranged from -50 to $0\,V$ with $10\,V$ interval. (b, d) I_D–V_G plots measured at a fixed V_D of $-50\,V$. (a, c) Data for GR-pentacene OFET and (b, d) data for Au-pentacene OFET.

plots showed G band at $\sim1580\,cm^{-1}$ and the 2D band at $\sim2680\,cm^{-1}$ with a small intensity of D band at ~1350 cm^{-1}. Small D band indicates a low level of defects or local disorder. The 2D/G intensity ratio was found as ~1.70 and 0.48 for top plot (monolayer graphene case) and bottom plot (multilayer graphene case), respectively.[13]

Figure 2 present a series electrical data to compare the graphene-electrode pentacene OFETs (denoted as GR-pentacene OFETs) and Au-electrode pentacene OFETs (denoted as Au-pentacene OFETs). Figures 2(a) and 2(b) are

the results for GR-pentacene OFET and Figs. 2(c) and 2(d) are the results for Au-pentacene OFET. The output characteristics (drain current versus drain voltage, I_D–V_D) were measured for gate voltage (V_G) ranged from -50 to $0\,V$ with $10\,V$ interval for devices with channel length of $50\,\mu m$ and width of $1\,mm$ are shown in Figs. 2(a) and 2(c). From these figures, it is clear that the performance of the OFETs was improved significantly with graphene electrodes. It was observed that the I_D of GR-pentacene OFET was much higher than that for Au-pentacene OFET. The pentacene film
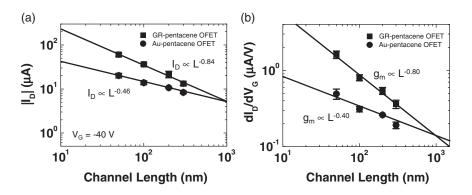
Fig. 3. Channel length dependence of (a) I_D (measured at $V_G = -40\,V$) and (b) transconductance for GR-pentacene OFET and Au-pentacene OFET. The error bars in (a) and (b) were obtained from measuring the standard deviation of about 5 devices at each data point.
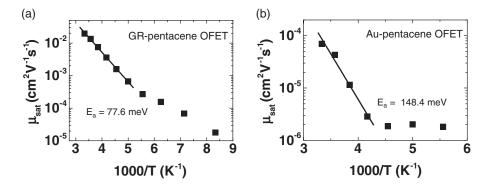

Fig. 4. Arrhenius plots of μ_{sat} values that were obtained at temperature from 300 to 210 K.

preparation condition of the OFET channel region is the same between the two types of devices. Therefore, the difference in the threshold voltage originates from the difference of injection property.[14] Similar to drain-induced barrier lowering (DIBL) mechanism in silicon MOSFET, different barrier heights from different electrode materials can affect the threshold voltage, as in our GR-pentacene OFET and Au-pentacene OFET cases. We have previously reported that the injection barrier height for GR- and Au-electrode OFET was found as ∼0.24 and ∼0.45 eV, respectively.[10] The improved performance of the GR-pentacene OFETs includes the effect of the pentacene in the contact region induced by the strong interaction of graphene with pentacene.[6]

The transfer characteristics (drain current versus gate voltage, I_D–V_G) for GR-pentacene OFET and Au-pentacene OFET are shown in Figs. 2(b) and 2(d), respectively. The field effect mobility was calculated in the saturation region at a fixed V_D of $-50\,V$ using

$$\mu_{sat} = \frac{2L}{WC}\left(\frac{\partial \sqrt{I_D}}{\partial V_G}\right)^2, \tag{1}$$

where W and L are the channel width and channel length, respectively, and C is the capacitance per unit area of the gate insulator. The μ_{sat} is often called as saturation mobility. Using eq. (1), we determined the μ_{sat} as ∼0.41 and 0.16 cm^2 V^{-1} s^{-1} for GR-pentacene OFET and Au-pentacene OFET, respectively. The on/off current ratio was high as 10^{-7} and 10^{-6}, for GR-pentacene OFET and Au-pentacene OFET, respectively. We also note that the GR-pentacene

OFET has better performance than Au-pentacene OFET, particularly in terms of the mobility.

We analyzed the two types of pentacene OFET devices in more details. Figure 3 show the data for I_D (measured at $V_G = -40\,V$) and transconductance ($g_m = dI_D/dV_G$ as a function of channel length for GR-pentacene OFET and Au-pentacene OFET. Through an empirical relationship of the power-law, the linear fits of I_D and g_m versus channel length (L) in the log–log plot were described as $I_D \propto L^{-\alpha}$ and $g_m \propto L^{-\beta}$, where α and β are fitting parameters of the scaling effect with respect to channel length.[15,16] The α value was obtained as 0.84 and 0.46 for GR-pentacene OFET and Au-pentacene OFET, respectively. When α becomes 1, $I_D \propto 1/L$, i.e., the drain current decreases as inverse of the channel length. In contrast, if α becomes less than 1, it means other effects such as contact resistance begins to influence the device more significantly.[16,17] Similarly, the β value was found to be 0.80 and 0.40 for GR-pentacene OFET and Au-pentacene OFET, respectively. Therefore, the results that much smaller α and β were achieved for Au-pentacene OFET suggest that the Au-pentacene OFET has larger contact resistance than GR-pentacene OFET, which is in accordance with the result of our previous study.[10] Note that we observed similar α and β fitting parameters for the data of I_D at different gate voltages.

The mobility is one of the key device parameters that represent the performance of the OFETs. Figure 4 shows the temperature-dependence of the μ_{sat} for GR-pentacene OFET and Au-pentacene OFET. The main feature here is that μ_{sat}

increased as temperature increased. In both device cases, there were temperature-dependent μ_{sat} region (at higher temperature range) and temperature-independent or weakly temperature-dependent μ_{sat} region (at lower temperature range). The temperature-independent μ_{sat} region can be dominated by tunneling mechanism and leakage currents,[18] which means charge carriers could not overcome the barrier height of bulk trap sites by thermal energy. On the other hand, the temperature-dependent μ_{sat} region can be interpreted by both thermal emission of carriers through Schottky barrier at electrode-pentacene contacts and thermal emission of charge carrier for a bulk conduction in pentacene.[19]

As shown the linear fit of Fig. 4, such typical temperature-dependent can be fitted by Arrhenius relation. The activation energy (E_{a}) can be calculated using[19,20]

$$\mu_{\text{sat}} \propto \exp\left(-\frac{E_{\text{a}}}{k_{\text{B}}T}\right), \qquad (2)$$

where k_{B} is Boltzmann constant.

From the slope of the logarithmic plot, the E_{a} of GR-pentacene OFET was found to be 77.6 meV and that for Au-pentacene OFET case was found to be 148.4 meV. The E_{a} of Au-pentacene OFET is about twice larger than that for GR-pentacene OFET. Note that we observed similar trend for the barrier height between the two types of devices.[10] The activation energy observed in Fig. 4 should be dominated by one of the two mechanisms with higher activation energy because it will be the rate limiting process. The activation energy for a bulk conduction in a pentacene layer was reported to be ~25 meV while the thermal emission at Schottky contact is higher than this value.[19] Therefore, the activation energy values observed in Fig. 4 can be attributed to the Schottky injection from the electrode to Pentacene with a barrier height proportional to the work function of electrode.[18] These results indicate that the graphene electrode has a lower barrier height-induced E_{a} value compared to that of the Au electrode case in pentacene OFETs.

4. Conclusions

In conclusion, we demonstrated that the performance of pentacene OFETs was enhanced by the use of multilayer graphene film as source and drain electrodes. The transport characteristics showed an improved mobility for pentacene OFETs with graphene electrodes as compared to the devices with Au electrodes. The channel length dependence of transport properties and temperature-variable mobility behaviors supported that the devices with the performance of graphene electrodes was enhanced due to contact resistance and barrier height lower than those of devices with Au electrodes.

1) G. Horowitz: Adv. Mater. **10** (1998) 365.
2) S. R. Forrest: Nature **428** (2004) 911.
3) H. Yan, Z. Chen, Y. Zheng, C. Newman, J. R. Quinn, F. Dötz, M. Kastler, and A. Facchetti: Nature **457** (2009) 679.
4) J. A. Nichols, D. J. Gundlach, and T. N. Jackson: Appl. Phys. Lett. **83** (2003) 2366.
5) M. Shtein, J. Mapel, J. B. Benziger, and S. R. Forrest: Appl. Phys. Lett. **81** (2002) 268.
6) C.-a. Di, D. Wei, G. Yu, Y. Liu, Y. Guo, and D. Zhu: Adv. Mater. **20** (2008) 3289.
7) C.-G. Lee, S. Park, R. S. Ruoff, and A. Dodabalapur: Appl. Phys. Lett. **95** (2009) 023304.
8) S. Lee, S.-J. Kang, G. Jo, M. Choe, W. Park, J. Yoon, T. Kwon, Y. H. Kahng, D.-Y. Kim, B. H. Lee, and T. Lee: Appl. Phys. Lett. **99** (2011) 083306.
9) Y. H. Kahng, S. Lee, M. Choe, G. Jo, W. Park, J. Yoon, W.-K. Hong, C. H. Cho, B. H. Lee, and T. Lee: Nanotechnology **22** (2011) 045706.
10) S. Lee, G. Jo, S.-J. Kang, G. Wang, M. Choe, W. Park, D.-Y. Kim, Y. H. Kahng, and T. Lee: Adv. Mater. **23** (2011) 100.
11) Y.-Y. Lee, K.-H. Tu, C.-C. Yu, S.-S. Li, J.-Y. Hwang, C.-C. Lin, K.-H. Chen, L.-C. Chen, H.-L. Chen, and C.-W. Chen: ACS Nano **5** (2011) 6564.
12) S. Pang, H. N. Tsao, X. Feng, and K. Müllen: Adv. Mater. **21** (2009) 3488.
13) X. Li, W. Cai, J. An, S. Kim, J. Nah, D. Yang, R. Piner, A. Velamakanni, I. Jung, E. Tutuc, S. K. Banerjee, L. Colombo, and R. S. Ruoff: Science **324** (2009) 1312.
14) S. Fukuda, H. Kajii, H. Okuya, T. Ogata, M. Takahashi, and Y. Ohmori: Jpn. J. Appl. Phys. **47** (2008) 1307.
15) G. Jo, J. Maeng, T.-W. Kim, W.-K. Hong, M. Jo, H. Hwang, and T. Lee: Appl. Phys. Lett. **90** (2007) 173106.
16) M. Noborio, Y. Kanzaki, J. Suda, and T. Kimoto: IEEE Trans. Electron Devices **52** (2005) 1954.
17) M. R. Pinto, E. Sangiorgi, and J. Bude: IEEE Electron Device Lett. **14** (1993) 375.
18) L. Diao, C. D. Frisbie, D. D. Schroepfer, and P. P. Ruden: J. Appl. Phys. **101** (2007) 014510.
19) H.-S. Seo, Y.-S. Jang, Y. Zhang, P. S. Abthagir, and J.-H. Choi: Org. Electron. **9** (2008) 432.
20) J. Chen, L. C. Calvet, M. A. Reed, D. W. Carr, D. S. Grubisha, and D. W. Bennett: Chem. Phys. Lett. **313** (1999) 741.